

Introduction

“While the founding fathers agonized over the question ‘particle’ or ‘wave’, de Broglie in 1925 proposed the obvious answer ‘particle’ and ‘wave’... [t]his idea seems to me so natural and simple, to resolve the wave-particle dilemma in such a clear and ordinary way, that it is a great mystery to me that it was so generally ignored.” -J. S. Bell

Quantum mechanics is perhaps one of the most counter-intuitive scientific theories in the history of the scientific method. At the atomic level, where quantum effects dominate, the laws that seem to govern our everyday world are no longer relevant. Determinism, the idea that every effect has a cause, is replaced with the idea that every action is probabilistic. A particle cannot be described by precise coordinates; instead, it is described using a wavefunction which provides a range of possible locations with associated probabilities. This probabilistic interpretation of quantum mechanics is known as the Copenhagen interpretation, and represents the most common form of rationalizing the radical, experimental observations of quantum mechanics.

In 2005, Couder et al. showed that oil drops bouncing on a vertically vibrated fluid bath exhibit properties analogous to the paradoxical properties previously seen only at the quantum scale [6]. The system operates at the macroscale, meaning that it is governed by the more “intuitive” classical laws, but still behaves *like* a quantum system. The accessibility of this experiment allows us to observe fundamental, “quantum”-like phenomena in a way that is impossible at the nanoscale. For example, in quantum mechanics, one can never know the position *and* the velocity of a particle, simply because it can never *have* a perfectly defined position and velocity. In this experiment, however, the “particle” can be easily seen at all times, so both its position and velocity can be easily tracked.

The behavior of the droplet system seems to agree with a theory of quantum mechanics proposed by Louis de Broglie in 1923 known as pilot-wave theory [7, 8]. Unlike the probabilistic viewpoint subscribed to by adherents of the Copenhagen interpretation, de Broglie’s model asserts that the particle *has* a precise location, and that the particle is pushed by a guiding or “pilot” wave. The theory was extended by David Bohm in 1952 [9, 10], but never caught on because it gained “realism” (the idea that a particle is well defined at all times) at the expense of “locality” (the idea of a universal speed limit where nothing, including information, can travel faster than the speed of light required by special relativity); a trade that is generally considered

unfavorable by physicists.¹

De Broglie's original theory is underdeveloped, having remained relatively obscure for the better part of the last century. Since the predictions of the Copenhagen interpretation and de Broglie's theory are similar, experiments have done little to clarify the debate. As a result, the more developed Copenhagen school of thought holds its place as *the* interpretation of quantum phenomena.

After taking a course in quantum mechanics, I found it difficult to truly believe some of the associated implications of the Copenhagen interpretation. I was seduced by some of the more obscure quantum methodologies that promised salvation from indeterminism and non-realism (such as Bohm or de Broglie's theories), and it was difficult from me to resist the opportunity to investigate analogs of these methodologies in an experimental setting. The bouncing droplet system, which serves as a hydrodynamic quantum analog and forms the backbone of this thesis, is introduced below.

Bouncing Droplets

Though it had been observed for at least a century, the phenomena of droplets bouncing on a fluid bath was first explained by Jearl Walker in 1978 [11]. The investigations began with a simple droplet of water falling onto a bath of water and remaining just a second too long before coalescence.² Walker discovered that by adding detergent to the water and vibrating the bath, he could extend the lifetime of the droplets from fractions of a second to several minutes. These droplets bounce at frequencies of around 50 Hz (50 bounces per second) and are very small, with a diameters of a millimeter or less. These two factors make it difficult to observe even the main mechanisms that drive the behavior. A key insight by Walker was that by flashing a strobe light at a frequency slightly slower than the rate of vibration of the bath, he could observe the droplet bouncing as if in slow motion.

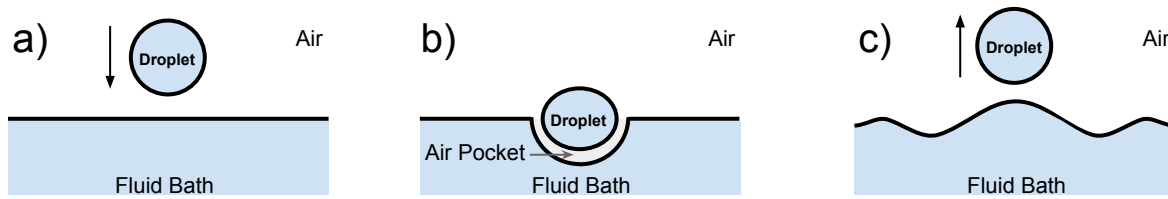


Figure 1: A depiction of a droplet bouncing on a bath of the same fluid. (a) A droplet falls onto a fluid bath. (b) A film of air gets trapped underneath the droplet. (c) The droplet bounces back up off of the cushion of air leaving behind waves that propagate radially.

Walker found that a trapped film of air kept the droplet and the bath from touching, as shown in Fig. 3. That is, the droplet is bouncing on a layer of air that is being pushed out from under the droplet, but because the bounce happens so quickly, the

¹The Copenhagen interpretation of quantum mechanics, by the way, is non-realist and non-local.

²It is often reported that this occurs in coffeemakers, as the coffee drips into the pot.

fluid droplet and the fluid bath never touch. Walker concluded that the leakage rate of this trapped pocket of air depends on three factors: the surface tension of the fluid in the bath, the viscosity of the droplet and the fluid bath, and the viscosity of air. He found that the bath must be of uniform surface tension and free from floating particulate matter, since both could lead to coalescence. Higher viscosity fluids led to longer droplet lifetimes, since more viscous fluids make it more difficult for air to escape the gap between the drop and the bath. Finally, adjusting the frequency and the amplitudes of the vibrations also affected droplet lifetime.³

More recent research showed that droplets of fluids like silicone oil can bounce indefinitely on a vibrating bath [2]. The long lifetime occurs not only because silicone oil has a high viscosity, but also because it has a *low* surface tension. A low surface tension is beneficial because it makes the oil bath relatively immune to surfactants (e.g. detergent) or contamination that would otherwise make the surface tension nonuniform and lead the drop to coalescence.

Faraday Waves

The behavior of a fluid in a vertically vibrated bath can be controlled by adjusting the amplitude or the frequency of the vibration. Depending on a variety of factors (size of bath, fluid in bath, etc.) each system has a specific amplitude (given a specific frequency), which if surpassed, will produce standing surface waves called Faraday waves [12].⁴ ⁵ A vibrating bath below this critical amplitude, also known as the Faraday threshold, will have a quiescent surface. A bath driven at an amplitude greater than the Faraday threshold will have a turbulent surface with ripples and waves. An example of Faraday waves is shown in Fig. 2. Adjusting the frequency above the Faraday threshold will change the size and shape of the Faraday waves. Note that Faraday waves can be created either by increasing the driving amplitude above a critical level, or adjusting frequency.

Walking Droplets

A bouncing droplet will bounce differently depending on the frequency and amplitude of the vertical vibrations. If the parameters are set just below the Faraday instability, a curious motion arises: the droplet seems to “walk” across the surface of the oil. The droplet is being pushed by its own ripples, a dual effort in which neither can exist without the other. In essence, the walker is both a particle and a wave; a conjunction reminiscent of the quantum scale.

³Reedie Andrew Case ('92) wrote his thesis “Oil on Troubled Water: The Extension of Floating Drop Lifetimes Due to Interface Vibration” where he looked at droplet lifetime as a function of vibrational frequency.

⁴Faraday waves were not actually discovered by Michael Faraday; in the footnotes of his paper he cites that they were first observed by Oersted, Wheatstone, Weber, and others. Faraday was just the first to study their behavior in detail.

⁵Another Reed thesis, this one titled “Good Vibrations: A Visual Exploration of Faraday Waves” by Alison Saunders empirically tested the mathematical Faraday wave model.

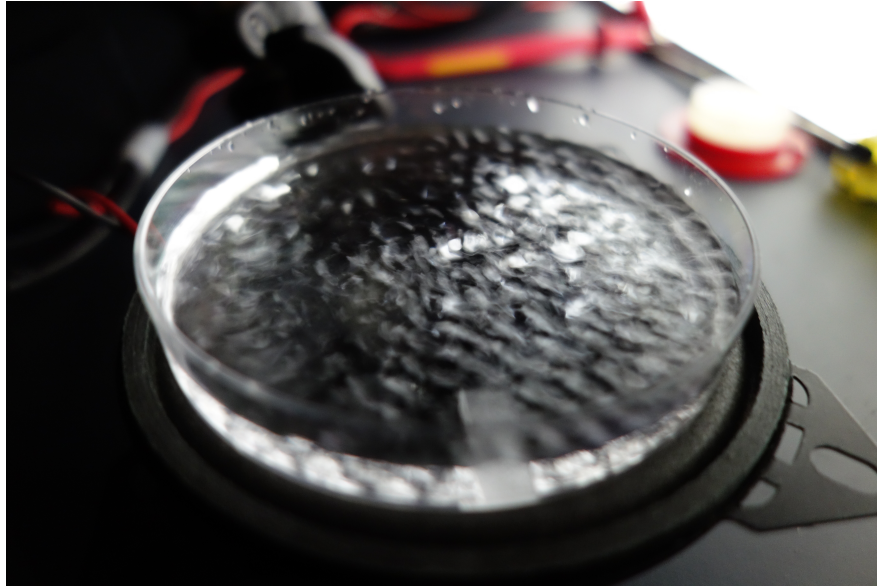


Figure 2: A picture of Faraday waves in a dish of water at 80 Hz.

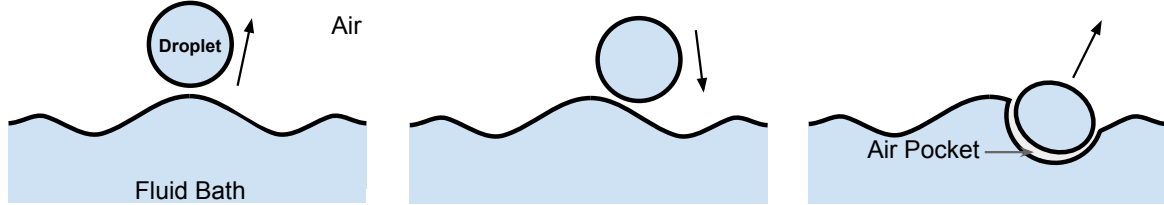


Figure 3: A depiction of a droplet walking across a bath of the same fluid.

Overview

Recently, two main groups have been investigating the properties of this unique system. A group at Laboratoire Matière et Systèmes Complexes (MSC) in Paris, France, headed by Yves Couder was the first to uncover some of the inherently “quantum”-like behavior of bouncing droplets, in 2005 [6]. Since 2010, John Bush’s group at MIT have created a mathematical model and performed their own investigations of the walker system. Couder, Bush, and others have shown that this system can reproduce double-slit single-particle interference [3], tunneling [5], quantized orbits [4], and many other “quantum”-like effects [1].

This thesis documents an experimental investigation into the “tunneling” behavior of this bouncing droplet system. In this setting, tunneling occurs when the droplet interacts with a submerged barrier. Only one other study looks at this aspect [5], but falls short of completely examining the tunneling behavior, focusing on the effect of barrier width and not examining barrier height. I hope to add to the body of work in this subfield by studying how barrier height affects probability of tunneling.

This thesis is divided into three main chapters. **Chapter 1** describes the hydrodynamic quantum analog along with a brief survey of the relevant literature. **Chapter 2**

Chapter 1

Pilot-Wave Hydrodynamics

In this chapter I will present a brief survey of the literature describing hydrodynamic quantum analogs, and discuss in more detail the tunneling experiments relevant to my investigation. Because the system was discovered in 2005, most of the literature examining this topic was written within the last decade.

1.1 Oil Droplet System

Consider a fluid of density ρ , viscosity ν , and surface tension σ in a bath of depth H . The bath is sinusoidally driven vertically with an amplitude A_0 at a frequency $f = \omega/2\pi$. By defining $\gamma = A_0\omega^2$, the effective gravity in the frame of reference of the bath is $g + \gamma \sin(\omega t)$. The surface of fluid in the shaking tray remains quiescent for lower values of γ . However, if γ is increased above a certain threshold (by increasing A_0 or f), the surface becomes unstable leading to the appearance of standing surface waves called Faraday waves. We define this threshold as the **Faraday threshold**, γ_F . The value of γ_F changes depending on the size and shape of the tray, the amount of fluid in the tray, as well as the properties of the fluid.

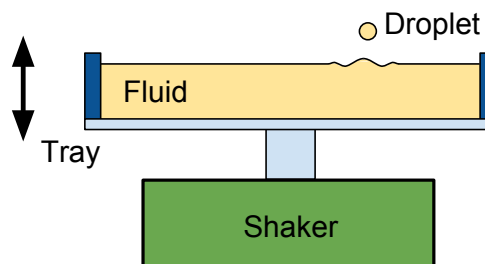


Figure 1.1: A droplet bounces on a vertically vibrating fluid bath. The tray vibrates with an amplitude A_0 at frequency f .

If we take a toothpick and break the surface of the vibrating oil bath, we form a droplet of oil of diameter D as shown in Fig. 1.1 that bounces on the surface for hours. The droplet bounces on a pocket of air, which is trapped beneath the droplet and the bath [11]. As the oil droplet bounces, it creates radially traveling waves that

propagate outwards on an otherwise flat surface. The droplet will continue bouncing for a specific range of values of γ . For small γ , the forcing is not enough to sustain the droplet, and it quickly coalesces. Increasing γ above the threshold for coalescence leads to a variety of different bouncing regimes until at $\gamma = \gamma_F$ where Faraday waves emerge. Below γ_F , the value of γ also affects the range of the radial waves; for low γ , these waves quickly dissipate, but as γ approaches γ_F , they are sustained longer. We are interested in studying the region below the appearance of Faraday waves but above the region of coalescence. The range of the various parameters which allow for the existence of bouncing droplets are outlined in Table 1.1.

Table 1.1: Approximate limits for bouncing drop behavior. The value $g = 9.81 \text{ m/s}^2$ is the standard acceleration due to gravity. Adapted from [1].

Parameter	Lower Limit	Upper Limit
Viscosity ν (cSt)	10	100
Bath Depth H (mm)	4	10
Frequency f (Hz)	20	150
Amplitude A_0 (mm)	0.1	1
Drop Diameter D (mm)	0.6	1.0
Forcing Acceleration γ (ms^{-2})	$0.5g$	$\gamma_F \approx 4.2g$

1.1.1 Faraday Waves

Driving a fluid-filled tray with forcing acceleration $\gamma = \gamma_F$ we see the appearance of standing surface waves known as Faraday waves. These waves oscillate with a frequency $f_F = f/2$ and an angular frequency $\omega_F = 2\pi f_F = \pi f$. For a fluid bath of density ρ , surface tension σ , and depth H , the standing wave and water dispersion relation:

$$\omega_F^2 = \left(gk_F + \frac{\sigma k_F^3}{\rho} \right) \tanh(k_F H), \quad (1.1)$$

can be used to find the wavelengths of standing waves at the Faraday threshold. This relates the angular Faraday frequency ω_F to the Faraday wavenumber k_F , where g is the gravitational constant [13]. From the wavenumber, we can calculate the wavelength λ_F of the Faraday waves by the relation $\lambda_F = 2\pi/k_F$. Though we are interested in investigating the region $\gamma < \gamma_F$ for which there are no standing surface waves, Eq. (1.1) provides an estimate of the wavelength and frequency of the localized waves surrounding the droplet for the bouncing behavior.

1.1.2 Vibration Number

In an experiment of this nature, one usually pours a specific volume of oil in the tray, fixing the values of ν , σ , and H . One is then left with the option to adjust γ

which produces a range of droplet motions, including a slew of different stationary bouncing modes and linear or chaotic “walking” trajectories (which are discussed in Section 1.1.3). To categorize the various bouncing behaviors, we use the vibration number V_i , which takes into account many of the parameters of the experiment [14]. The vibration number is the ratio of the forcing frequency and the droplet’s natural oscillation frequency ω_D and is given by:

$$V_i = \frac{\omega}{\omega_D}. \quad (1.2)$$

where ω_D represents the oscillation frequency of a fluid droplet. Rather than remain a perfect sphere, the droplet stretches and contracts vertically as it bounces, and ω_D describes the frequency of this motion. The oscillation frequency of a fluid droplet is defined as:

$$\omega_D = 2\sqrt{\frac{2\sigma}{\rho D^3}}, \quad (1.3)$$

where σ is the surface tension, ρ the density, and D the diameter of the droplet [15]. Combining Eqs. 1.2 and 1.3 we arrive at:

$$V_i = \frac{\omega}{2} \sqrt{\frac{\rho D^3}{2\sigma}}, \quad (1.4)$$

a dimensionless parameter that captures the effects of the fluid’s material properties, the tray’s vibration, and the droplet’s diameter. Depending on the vibration number V_i and the driving strength γ/g , the droplets switch between different bouncing states as shown in Fig. 1.2. If we hold the working fluid and the driving frequency constant (σ , ρ , and ω), then we can think of increasing V_i as increasing droplet diameter D .

The various modes seen in Fig. 1.2 can be described by a pair of numbers m and n , where n is the number of times the droplet contacts the surface over a time span m/f . For example, in the (1,1) “bounce” mode, the droplet hits the oil bath once per up-and-down motion of the tray. In the (2,2) mode, the drop makes two bounces of differing heights for two driving periods. The “chaos” regimes indicate that the bouncing of the droplet is chaotic and does not exhibit a periodic bouncing motion. The “walk” regime describes a very particular kind of behavior in which the droplet moves forward as it bounces, seemingly walking across the surface. Like bouncing, walking also comes either the (2,1), (4,2), or chaotic modes. Finally, the “coalescence” region demarcates the values for which the droplet coalesces with the bath.

The phase diagram shown in Fig. 1.2 provides a valuable starting place for an experiment since it outlines the many possible states of the system, and where we can expect to find particular behaviors. We will now narrow our focus to only the walking regime, which is the focus of this thesis.

1.1.3 Walking

A walking droplet is a very specific type of bouncing droplet that arises between $\gamma_W < \gamma < \gamma_F$, where γ_W the the walking threshold. As the droplet bounces vertically

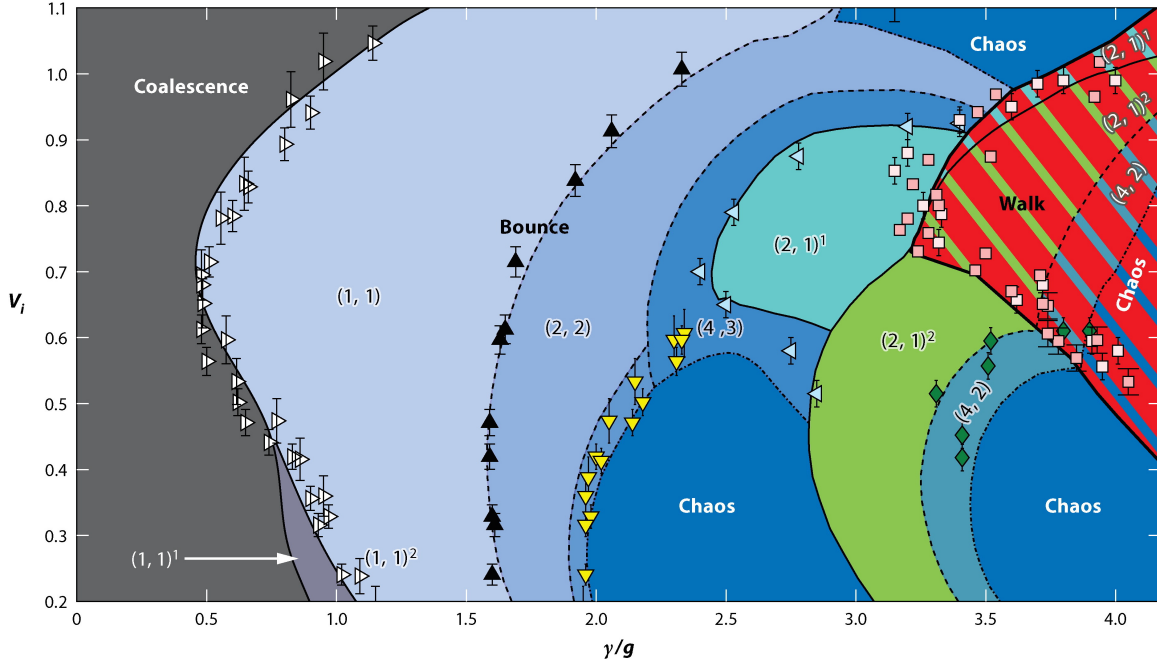


Figure 1.2: The different bouncing regimes for the oil drops of 20 cSt silicone oil at $f = \omega/2\pi = 80$ Hz, characterized by the non-dimensional forcing amplitude γ/g and the vibration number V_i . The solid colors represent the modes predicted by a theoretical model [14], and the various points represent experimentally measured limits. The parameters $(m, n)^i$ describe a droplet that bounces n times in m forcing periods, where i distinguishes modes with different mechanical energy. The Faraday threshold is $\gamma_F = 4.2$. Adapted from J. W. M. Bush, Annu. Rev. Fluid Mech. **47**, 273 (2015).

on the vibrating fluid bath, the interaction with the wave it generated during its previous bounce gives it a slight horizontal motion. Thus, for every bounce, the droplet follows a parabolic trajectory. But because these droplets are bouncing at 40 times per second (or more) and the parabolic motion is periodic, the vertical oscillations are difficult to see. The apparent behavior that emerges is that of the droplet moving in a straight line along the surface of the fluid bath.

The horizontal component of the walking motion is due to the droplet landing slightly off center from the radial wave it produced in the previous bounce, as shown in Fig. 1.3. At such close proximity to the Faraday threshold, the waves surrounding the droplet are not just regular ripples, but rather are like localized Faraday waves temporarily sustained by the vibrations before decaying away. The kinetic energy from the falling droplet is enough to perturb the unstable surface such that the waves appear, and then the energy introduced by the vertical forcing of the tray keeps these waves from damping out completely, as they would in an un-forced system. The value of γ determines how long these local Faraday waves are sustained. As these waves interfere with one another they create an overall wave field that guides the droplet. This overall wave field is referred to as the **guiding wave** or the **pilot wave**. A

droplet's location over time (discussed in Section 1.2.1) [8]. The second statistical wave describing the long term motion of the particle in de Broglie's theory is the very same wave that describes the particle's probable location using the Copenhagen interpretation, but because of de Broglie's extra pilot wave, the same wave is interpreted differently. Unfortunately, because de Broglie could never find the equation of the pilot wave, he could not proceed with his theory and it fell into obscurity. His theory was picked up and modified by David Bohm in 1952 [9, 10], who combined the statistical wave and the guiding wave into a single wave. By combining the two waves, Bohm's formulation loses its relevance to the bouncing droplet system.

It is worth noting that there are a few differences between the hydrodynamic system and an actual quantum system. First of all is the scale; the bouncing droplet system moves under the laws of the macroscopic world. Secondly, the hydrodynamic system is dissipative (waves are damped) and sustained only through continuous energy input (constantly being vibrated), so it is not a conservative system. With that said, it is still worth comparing the two since they appear similar in many other respects.

Despite these differences, it is worth investigating the hydrodynamic pilot-wave analogs in greater detail. We will narrow our focus once again, and investigate the tunneling behavior of this system, which describes the droplet's interaction with subsurface barriers. The following section explains tunneling in quantum mechanics, and the analogous behavior in the droplet system.

1.2.1 Long Term Droplet Behavior

Constraining a walker to a circular region, Harris et al. tracked the motion of the walker over a long period of time [20]. In the high-memory, chaotic motion regime, the droplet was allowed to walk freely while its position was tracked (Fig. 1.6(a)) and translated into the histogram (Fig. 1.6(b)). The histogram provides the probability of finding the walker at a specific location within the corral, and recovers the shape of the Faraday wave that occurs at the Faraday threshold. This histogram serves the same purpose as de Broglie's statistical wave described by the Schrödinger equation. In the Copenhagen interpretation of quantum mechanics, however, this statistical wave (called the wavefunction) fully defines the particle.

1.2.2 Tunneling

Tunneling in Quantum Mechanics

Among the various phenomena associated with quantum mechanics, tunneling is one of the most surprising. At the classical level, we can take the example of a basketball thrown at a brick wall: the ball will hit the wall and bounce back every time we try it. When we shift to the quantum scale, if we have a particle headed towards a barrier of a given potential energy, it will not necessarily bounce back. Depending on the characteristics of this potential, there will be a few times in which the particle will **tunnel** through the barrier, shooting out on the other side. It is not completely fair

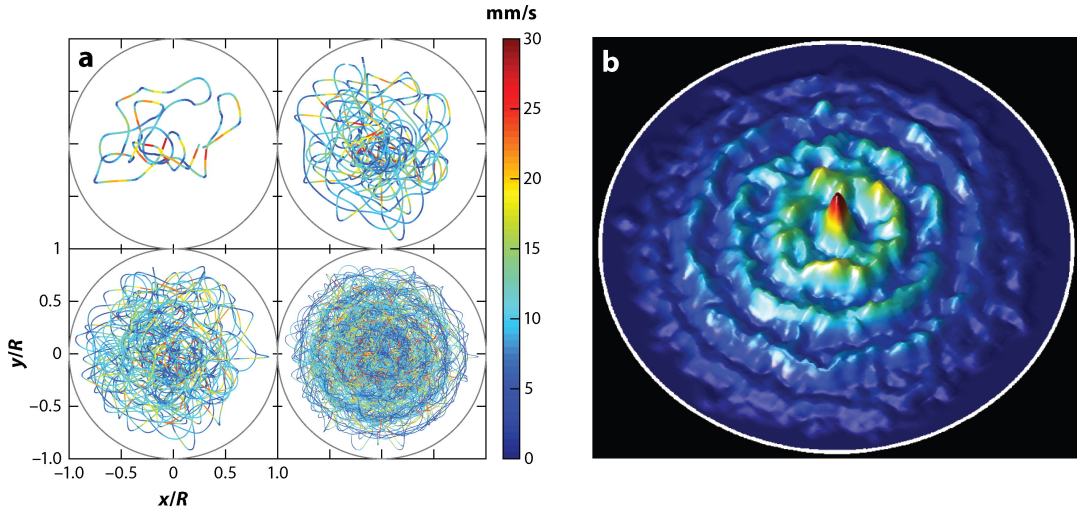


Figure 1.6: The figures show the motion of a single chaotic walker in a confined circular geometry. In (a) the path of the moving droplet is traced, where color indicates the velocity of the droplet. In (b) a histogram shows the droplet’s position within the circular corral over a span of time. A clear pattern emerges: the droplet appears to be contained within a statistical wave of wavelength λ_F . Adapted from J. W. M. Bush, Annu. Rev. Fluid Mech. **47**, 275 (2015).

to use the basketball/wall example as an analogy for the particle/barrier interaction because the “effective potential energy” of the brick wall is almost infinite, while that of the quantum potential barrier that allows tunneling, is not. For a high enough potential, the particle will also (almost) always bounce back. The point is that probabilistic tunneling cannot be seen at a classical scale in the way that is at the quantum scale, at least not until the discovery of the bouncing droplet system.

Tunneling in the Bouncing Droplet System

A study performed by Eddi et al. examined tunneling in the bouncing droplet system [5]. In this setting, tunneling takes the form of the droplet tunneling through (or being reflected by) a submerged barrier. The droplet never actually travels through the barrier, since it bounces on the interface, but the analog to quantum tunneling remains because as the droplet approaches the barrier it is affected by the region of a different “potential”.

For a different depth of fluid H , a tray will have a different γ_W . If a tray has various regions of different depths, then these different regions will behave slightly differently. This means that when a walker travels from an area of one depth to an area of another depth, its behavior may change. This effect can be seen when a walker is pushed back from a submerged step, seemingly without any contact with the droplet. However, in certain cases, the walker will actually “tunnel” across the step; that is, it will continue to walk along the surface of the oil bath and pass into the new region of different depth, without reflection. Adjusting the width of the barrier as well

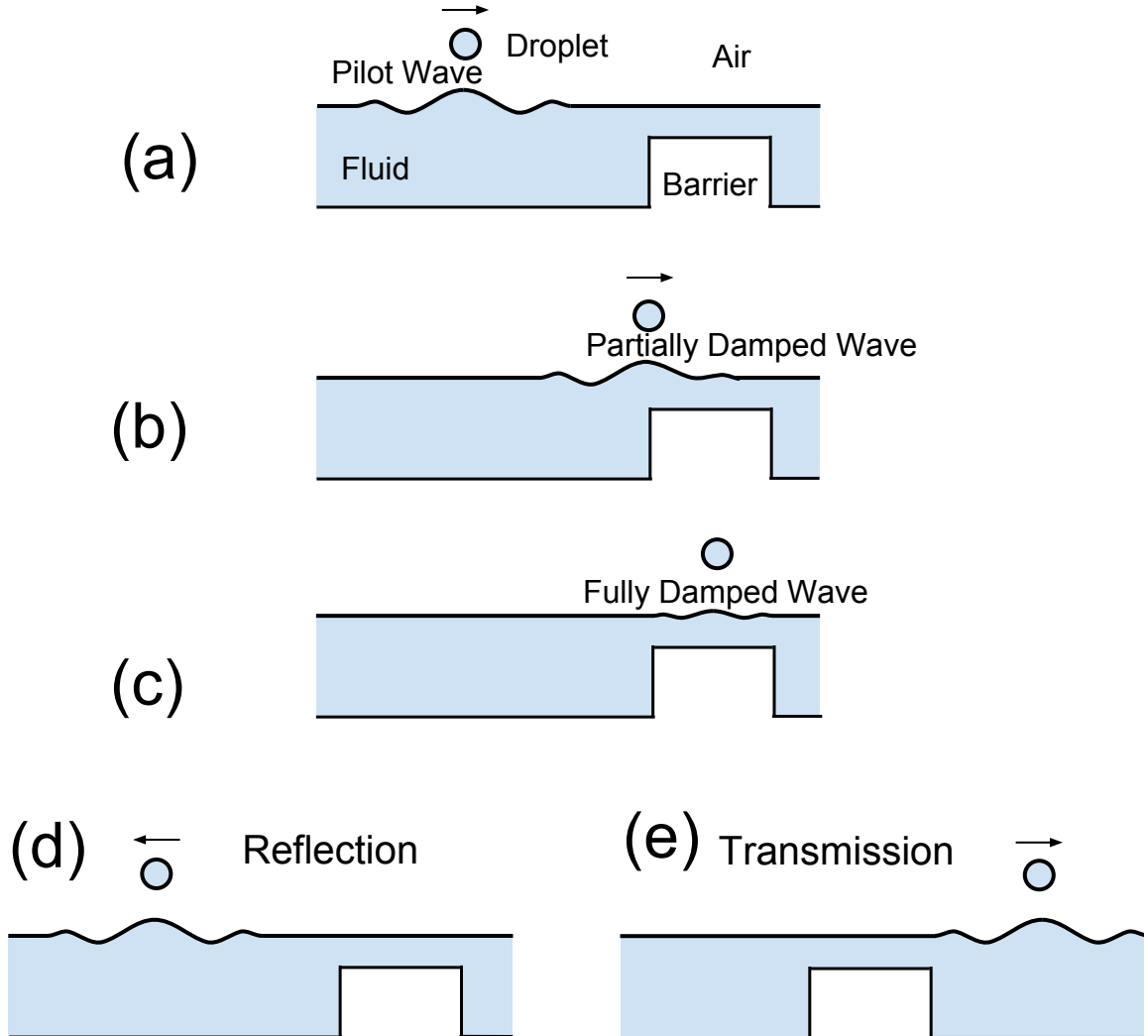


Figure 1.7: A diagram of the droplet-barrier interaction. In (a) the walker moves towards the barrier. As it gets closer (b), the guiding wave is damped. In (c) the guiding wave is fully damped such that the droplet is no longer a walker but a bouncer. Guided by the waves the droplet generated as a walker, the bouncer will either be reflected back from where it came (d), or carry on as shown in (e).

as its height will affect the behavior of the droplet. If we make the barrier of width e with height such that the depth of the oil above it is h , in a bath that otherwise has depth H , then we can think of it as a potential barrier. The unpredictability of the tunneling comes from the complex interaction between the drop and its guiding wave.

Now say we set γ such that walking occurs in the deeper section, but not in the more shallow section (i.e. $\gamma_w(H) < \gamma < \gamma_w(h)$). Then, the droplet is simply a bouncer when in the shallow region, but a walker everywhere else. If the droplet starts out in the deeper region but crosses over to the shallow barrier, it slows down since it is no longer generating the self-propelling waves required for the walking

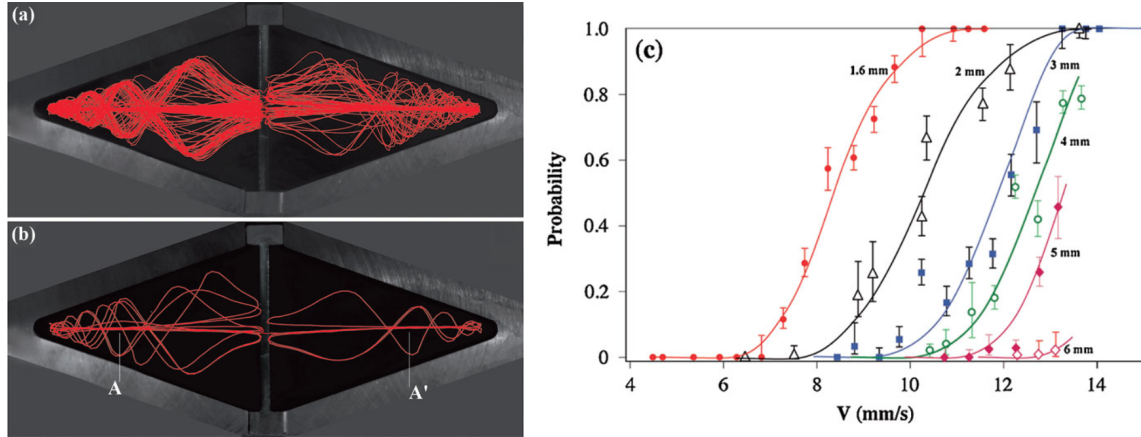


Figure 1.8: In (a) and (b) we see the path of a droplet traced out over many collisions with the barrier within rhombus shaped tray. The plot (c) shows the tunneling probability as a function of walker velocity for different barrier widths. Figures adapted from A. Eddi et al., Phys. Rev. Lett. **102**, 240401 (2009).

motion. Instead, the superposition of previous waves is what guides it either through or away from the barrier. However, if a droplet were to be created on the barrier, it would remain motionless. Therefore, we can understand the act of tunneling proceed as follows: the walker approaches a barrier, crosses the barrier as a bouncer, and eventually returns to the deeper region as a walker. The process is depicted in Fig. 1.7.

Eddi et al. built a tray with a submerged rhombus shape which forced the walker across the center of the tray as shown in Fig. 1.8 (a) - (b) [5]. A barrier was then placed along the diagonal of the rhombus, perpendicular to the direction of travel of the walker, so that the walker would run directly into the wall. They showed that as γ/γ_F approached 1, faster droplets had higher probabilities of tunneling (Fig. 1.8 (c)). They also discovered that by increasing the barrier width, the tunneling probability decreased.

The question that lingers, and that is the focus of this thesis, is the following: **How does tunneling probability change as a function of oil depth above the barrier h ?** We expect that at large h values the localized Faraday waves will be less damped, meaning that the walkers will tunnel more frequently. At small values of h where the localized Faraday waves are heavily damped, it is predicted that there will be very little tunneling. What is the critical height where we see both behaviors? An experiment, detailed in the following chapter, was designed to test this question.

Chapter 2

Experimental Design

In the bouncing droplet system we observe a unique interaction between a droplet and its wave that showcases various novel behaviors under different circumstances. In the experiments discussed herein, we will look at how features submerged beneath the surface of the oil affect the motion of the droplet.

A raised object on the floor of the tray (but still underneath the surface of the oil) can have an effect on height of the surface waves, and thus, on the motion of the walker [5]. Sometimes a droplet headed towards a raised object will be reflected backwards, as if from a collision with the object. For this reason, we refer to a submerged object as a barrier.

Oftentimes however, the droplet slows down, but continues on and crosses over the barrier without a collision. This is analogous to “transmission” in the quantum mechanical process of tunneling. For a barrier of a given height and width, there is a probability of tunneling unique to that barrier. Earlier studies have shown that increasing barrier width decreases probability of tunneling [5]. This study looks at how the height of the barrier affects the tunneling probability.

To test the effect of a barrier’s height on the probability of tunneling, I used a combination of procedures from the investigations of Bush et al. [1], Couder et al. [2], and specifically, Eddi et al. [5]. These were slightly modified to fit some of the unique features of my experiment. In this section, I aim to give some of the reasoning behind the design of the experimental apparatus and data collection techniques, both of which are not well described in the literature.

2.1 Setup

To guide the discussion of my experimental design, a schematic of the experimental setup is shown in Fig. 2.1 and a picture of the actual setup is shown in Fig. 2.3(a). In the experiment, a waveform generator creates a sinusoidal signal which is amplified and fed into a shaker. This signal drives the shaker, which vertically vibrates the tray containing the fluid. Both the frequency and the amplitude of the vertical oscillations can be controlled. An accelerometer records the vertical acceleration of the tray and is read using an oscilloscope. A CCD camera is used to record the droplet as it bounces

along the surface of the oil.

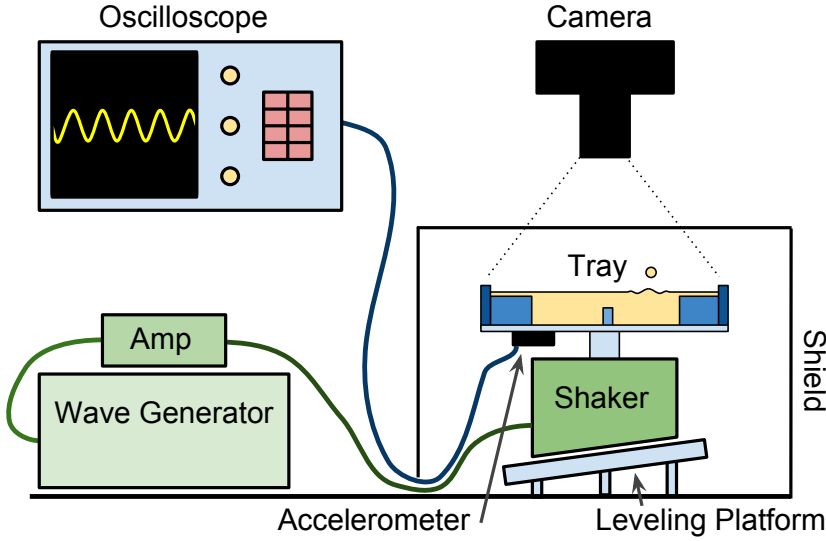


Figure 2.1: The experimental setup. The amplified signal from the wave generator drives the shaker, which shakes the oil-filled tray. The accelerometer generates a signal, which is read by the oscilloscope. The shield blocks disturbances to the experiment, while allowing the camera to document the trials.

2.2 Materials

The key components of this experiment are the shaker, the oil, and the tray. In this section I will describe the specifics of this holy trinity, as well as some of the additional components used in data collection.

2.2.1 Tray

The tray's design, which was based off of the tray in the tunneling experiment of Eddi et al. [5], naturally guides the droplet into a perpendicular collision with the barrier. The tray was fabricated from acrylic plastic parts that were cut on the Trotek Rayjet 300 laser cutter in Reed's machine shop. The manufactured components were then glued together with Scigrip Weld-On 3 assembly adhesive. A detailed schematic of the tray is shown in Fig. 2.2.

A thin layer of oil spills over the constraining rhombus shape. As long as the layer is thin enough, the droplet will remain in the rhombus container, but the waves will continue to propagate unimpeded. This gives the waves time to decay, meaning that the droplet's motion is not affected by reflections of previous waves from the sidewalls, and is instead guided only by the unreflected waves. The rhombus shape serves to steer the droplet into a perpendicular collision with the barrier. It does this by forcing the droplet to pin-ball into the acute corner of the rhombus so that it shoots out towards the barrier as shown in Fig. 2.3(c).

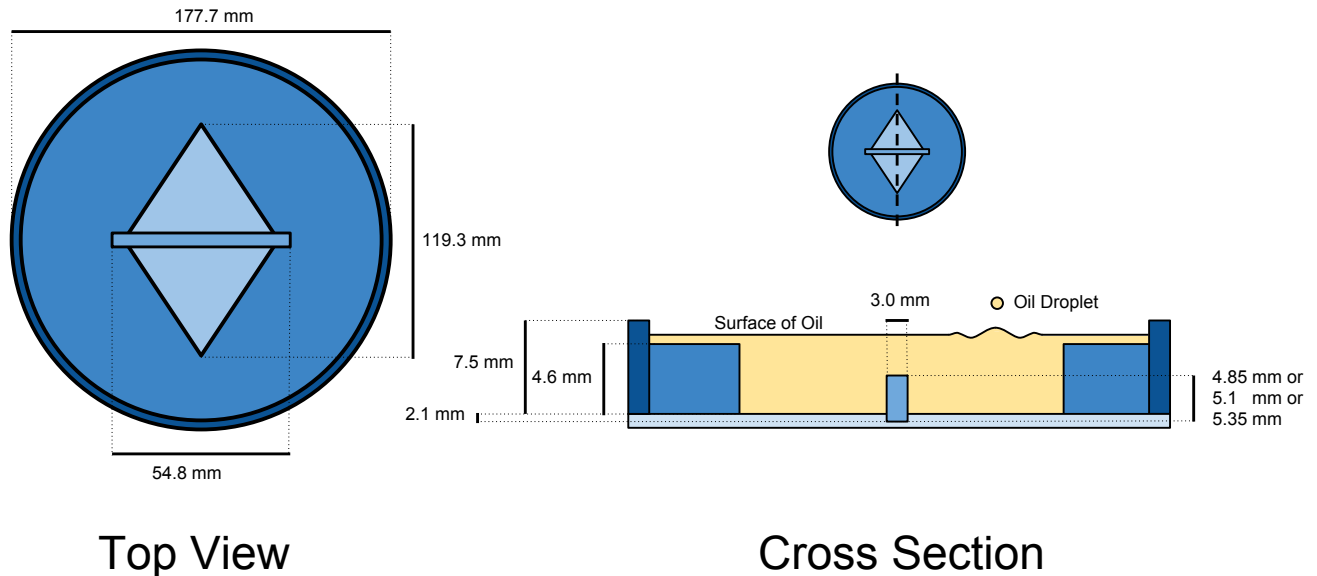


Figure 2.2: The specifications of the tray design. The top view (left) highlights the main elements in the tray. The cross section (right) illustrates the topography of the tray. The depth of the fluid layer is represented by the shading; darker shading is shallower.

We designed the experiment to test barriers of three different heights: 2.75 mm, 3.0 mm, and 3.25 mm, measured from the bottom of the rhombus. Thin acrylic barriers made by the laser cutter have a tendency to bend and warp over time. To avoid this problem, we made the barriers taller than the specified heights. Then we created a cut-out in the bottom of the rhombus so the barriers could be inserted and held in place by the tight fit. The barrier cut-outs were deep enough to exactly counter the added height of the barrier, so the barriers still had (when measured from the surface of the rhombus) heights of 2.75 mm, 3.0 mm, and 3.25 mm. This design also solved the problem of fixing the barriers in place, while allowing them to be easily removed. The particular heights of the barriers were chosen because they exhibited both transmission and reflection. Other barriers were also made but these were either too tall (3.5 and 4.0 mm) and blocked all of the droplets, or too short (1.0 and 2.0 mm) and did nothing to prevent the droplets from crossing over.

In order to improve contrast, the bottom of the tray was painted black, allowing the droplet to be more easily tracked by eye and when using a camera.

2.2.2 Silicone Oil

Silicone oil was the ideal choice of fluid for this experiment because it remains clean, it has a low vapor pressure (so it does not evaporate), and it can be purchased in a range of specific viscosities. The silicone oil used in this experiment had a viscosity of 20 centistokes (cSt) (its viscosity is a little closer to water than olive oil) and was purchased from Clearco Products Co. Inc., Bensalem PA (CAS No: 63148-62-9). 20

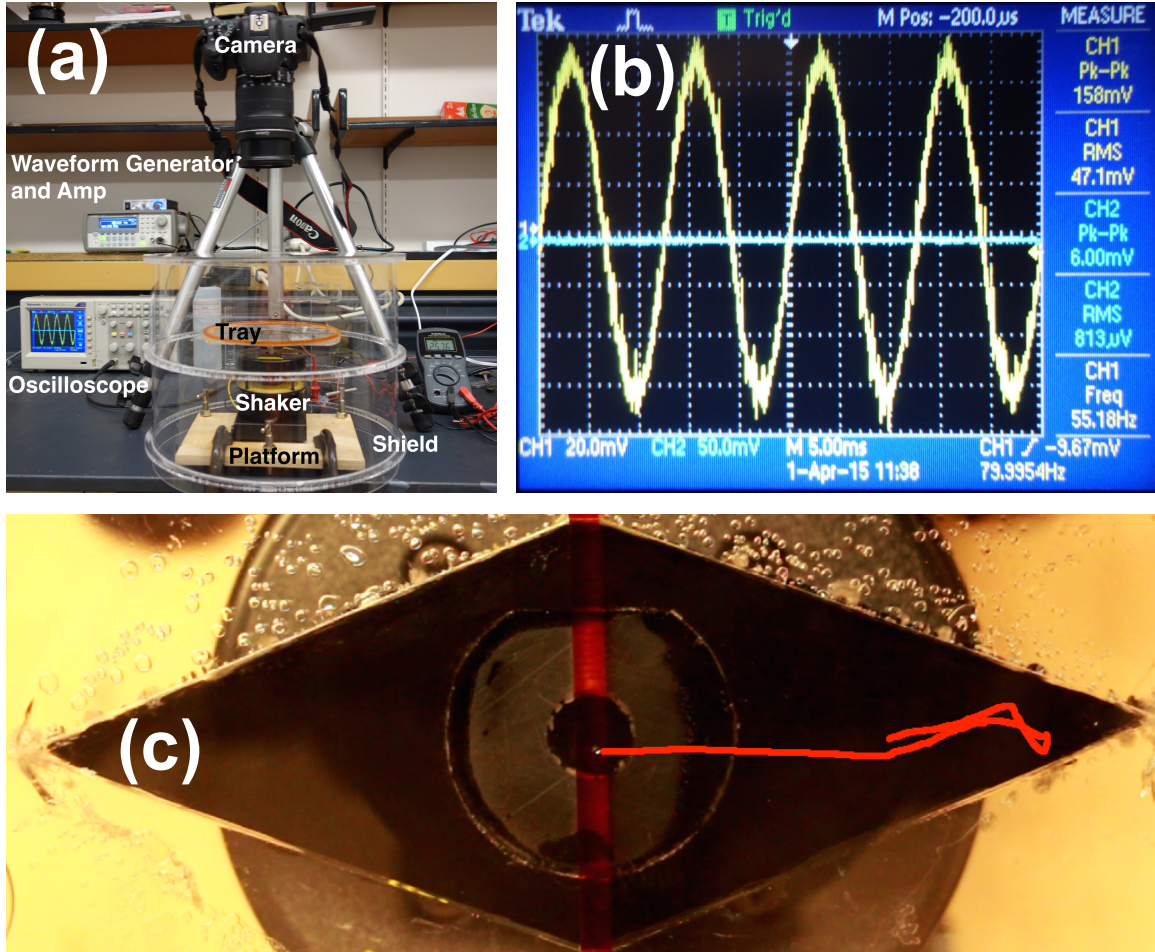


Figure 2.3: (a) The actual experimental setup. (b) The screen of the oscilloscope, showing the output from the accelerometer. The sine wave is proportional to the acceleration of the tray and has a frequency of 80.0 Hz and a peak to peak voltage of 158 mV. (c) The path of a droplet with a diameter of 0.87 mm, highlighted in red, shows the droplet's motion as it walks into a corner before shooting out directly towards the barrier (orange).

cSt silicone oil, like the one used by Bush et al. [1] was chosen because it exhibits walking behavior over a wider range of parameters [1] than more viscous oil, such as the 50 cSt viscosity oil used by Couder [2]. Depending on the height of the barrier and the desired height of oil above the barrier, the tray requires approximately 18.0 mL of fluid. This volume of oil left a different depth of oil above the barrier, depending on which barrier was in place. For the shortest barrier of 2.75 mm, the depth of the oil on top of the barrier was 1.5 mm. The intermediate barrier of height 3.0 mm had about 1.25 mm of fluid above it. The tallest barrier at 3.25 mm, only had 1.0 mm of fluid on top. The depths of the oil were calculated using the known oil volume and the dimensions of the tray.

It was of vital importance to keep the oil as clean as possible since surface contamination leads to droplet coalescence. This meant protecting the oil from particulate

$$h_{2.75} = 1.51 \pm 0.04 \text{ mm}$$

$$T_{2.75} = 17/17 = 1.0$$

$$h_{3.0} = 1.26 \pm 0.04 \text{ mm}$$

$$T_{3.0} = 7/19 = 0.37$$

$$h_{3.25} = 1.02 \pm 0.03 \text{ mm}$$

$$T_{3.25} = 0/18 = 0.0$$

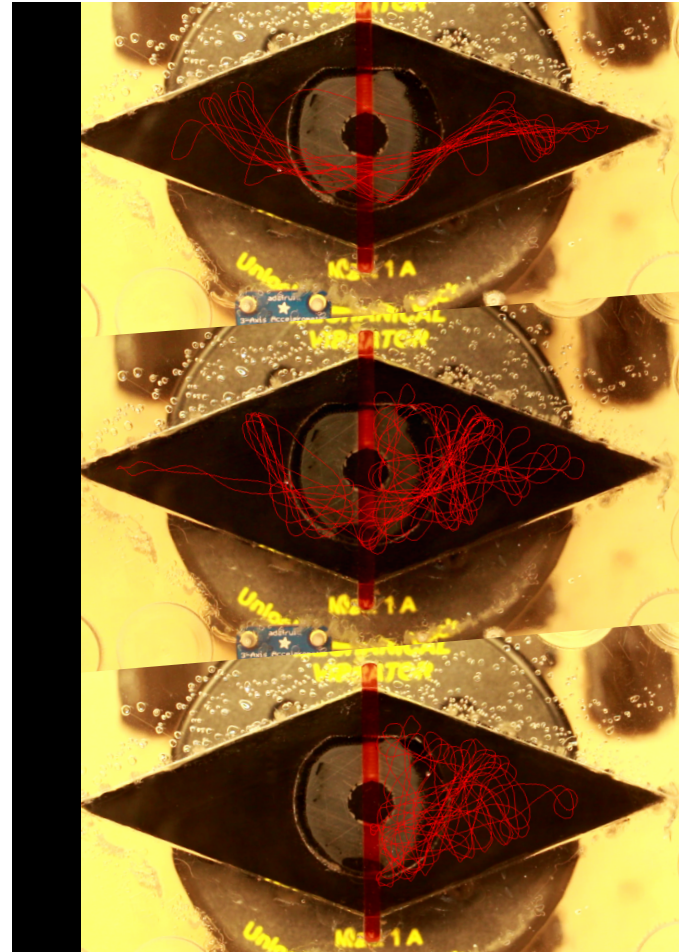


Figure 3.1: The raw data from Trial 2. The red line in each image traces the path of the droplet for the duration of the trial. For each of the three barrier heights, the depth h of the oil above the barrier is shown, along with the fraction of droplets T that tunneled across the barrier.

indicating that droplets never crossed near $h = 1.0$ mm, whereas they always crossed at $h = 1.5$ mm. For the intermediate depth $h = 1.25$ mm, both transmissions and reflections were observed at a rate that changes for every trial. If we consider the droplet diameter, we see that the plot suggests that the transmission coefficient increases as the diameter of the droplet increases.

3.2.2 Tunneling by Droplet Velocity

Not every droplet barrier collision was ideal. Many times, the droplets approached at an angle or at different velocities which means that it is misleading to consider every collision as being the same. One way we can standardize collisions is by looking at the velocity perpendicular to the barrier at 5 mm away from the center of the barrier, as shown in Fig. 3.3.

We expect the perpendicular component of velocity to be important because it

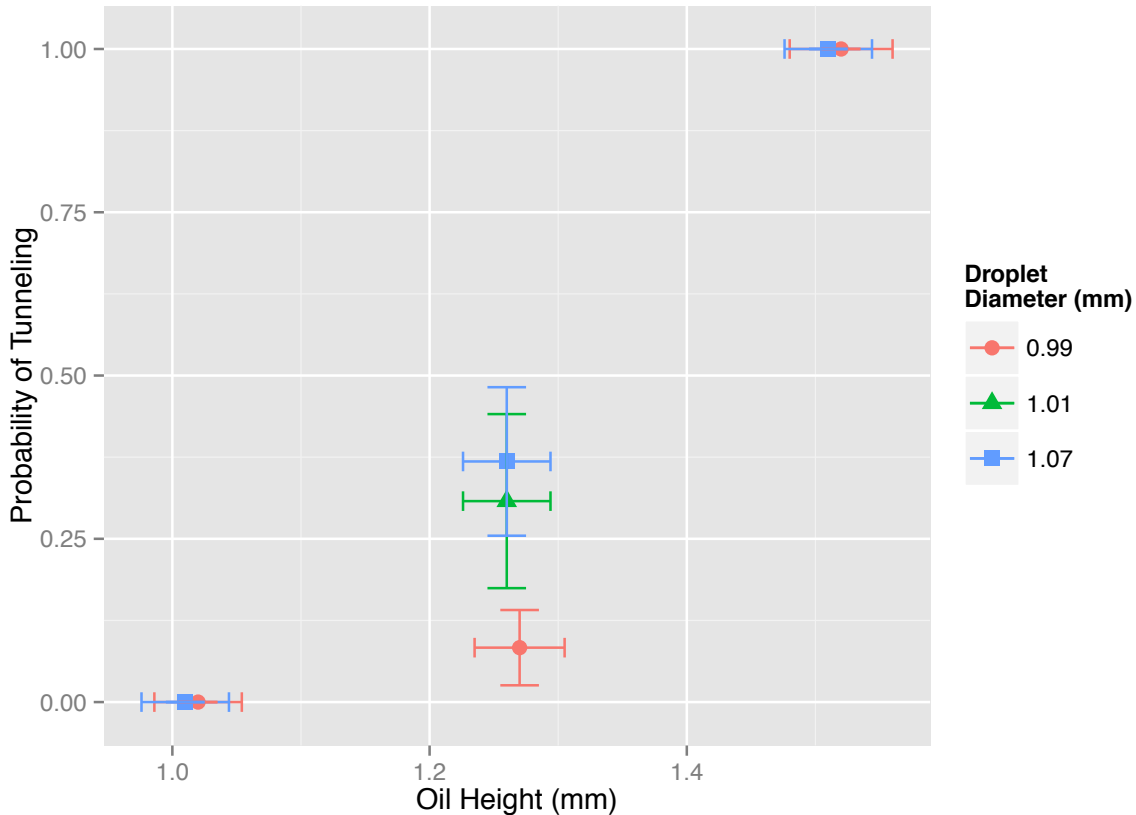


Figure 3.2: The proportion of collisions leading to transmission as a function of h . Each data series corresponds to a single trial for which the droplet diameter was kept constant. The vertical error bars indicate standard error, and the horizontal error bars indicate uncertainty calculated using error propagation.

proved critical in the study of barrier width carried out by Eddi et al. [5], and because intuitively, if the droplet moves faster, it has greater momentum and is more difficult to stop. Fig. 3.4 shows every collision for the intermediate barrier height, and the result of each interaction. In trials 2 and 3, the droplets with the fastest perpendicular velocities were usually the ones that passed through the barrier, as expected. This did not seem to be the case for trial 1, for unknown reasons.

Next, we try breaking up the collisions by velocity. The collisions from the 3.0 mm barrier were grouped into bins of width 2 mm/s and plotted by the fraction of all collisions that tunneled. The result, shown in Fig. 3.5, leaves a little to be desired. We see immediately the major limitation is the lack of trials, and perhaps, in consistency. Trial 3 is the only one that shows the expected trend for all bins: as velocity increases so does tunneling. Trial 2 starts off on the right track but a few reflections at high velocities skew the results. Finally, the results from trial 1 are inconsistent with the predicted behavior.

Our data seem to indicate that tunneling probability increases as a function of velocity and of droplet diameter. Droplet diameter is really just a way of expressing

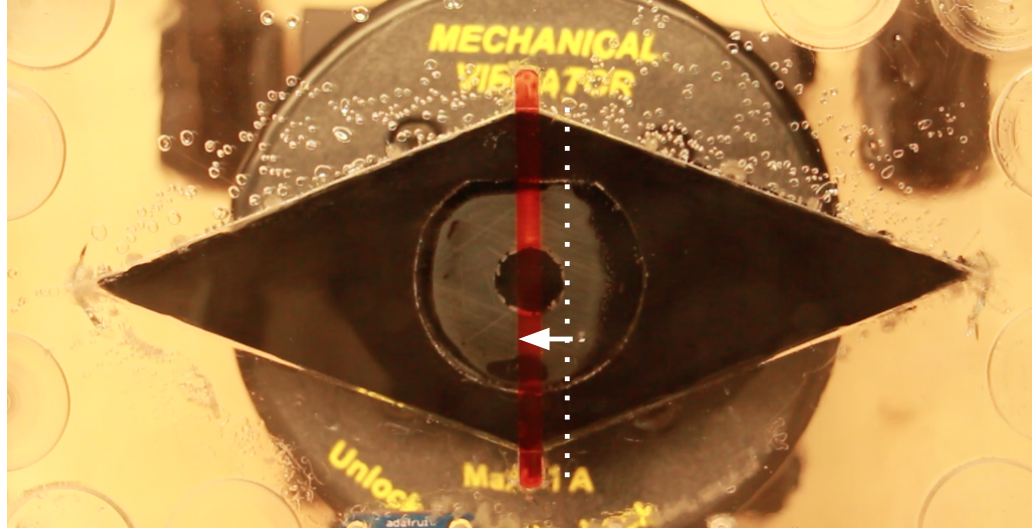


Figure 3.3: The image shows the point at which the measurement of the perpendicular component of velocity was made. This is 5 mm from the middle of the barrier.

the size of the droplet, but another way of doing that is by using the droplet's mass m . The momentum p of an object of mass m and velocity v is defined as:

$$p = mv.$$

We can estimate the mass of the droplet by multiplying the volume of the droplet by its density ρ . Assuming a spherical droplet of diameter D , the volume is given by:

$$V_d = \frac{4}{3}\pi \left(\frac{D}{2}\right)^3.$$

Thus, we can express the momentum of the droplet as

$$p_d = \rho V_d v \quad (3.1)$$

$$= \rho \frac{4}{3}\pi \left(\frac{D}{2}\right)^3 v \quad (3.2)$$

where the density ρ of silicone oil has been provided by the manufacturer. Looking at just the perpendicular component momentum and grouping the droplets into bins (as we did in Fig. 3.5 and then multiplying by the calculated mass m of the droplet) and we get the plot shown in Fig. 3.6. The plot shows incredibly similar slopes for portions of trials 2 and 3, suggesting the importance of momentum as a factor that increases tunneling probability. Even one of the momentum bins from the first trial falls on the curve, though the rest of the bins from that trial remain unexplained.

3.3 Sources of Error

With a system like the one studied here, which is sensitive to small variations in any parameter, it is crucial to keep track of the errors so that we can consider the

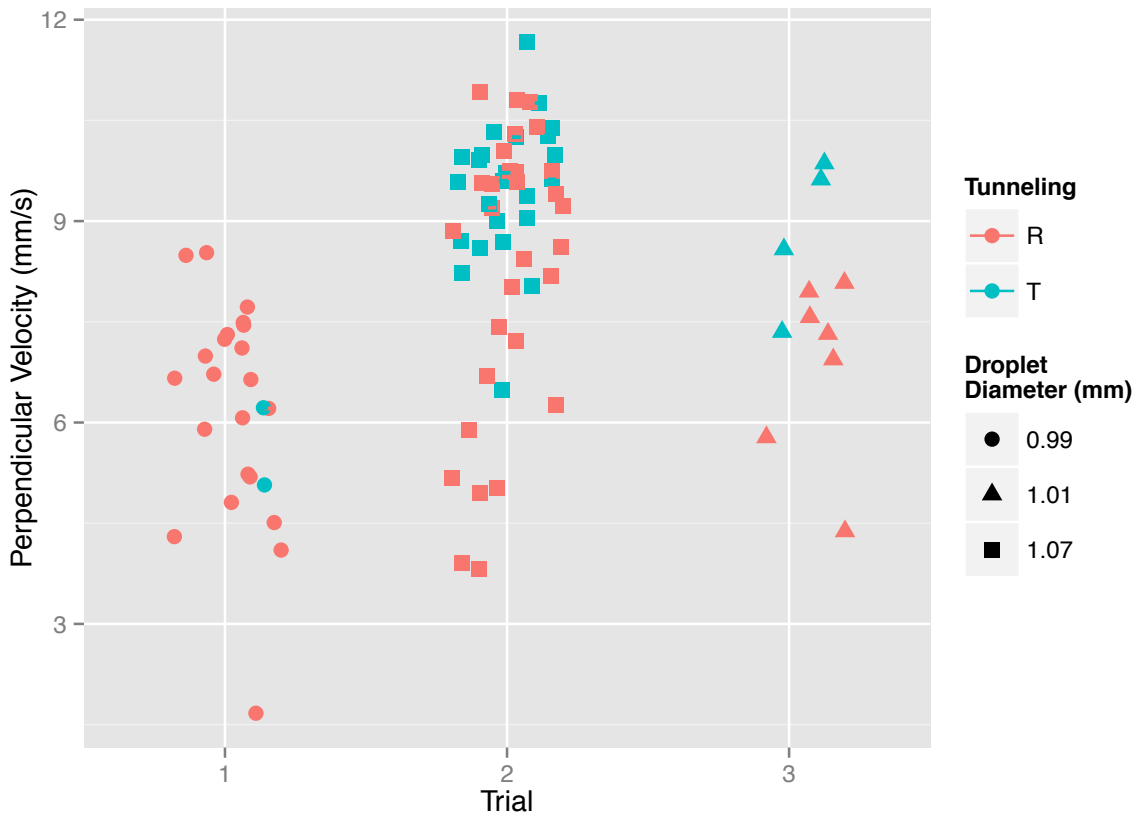


Figure 3.4: The result of each collision for the intermediate oil depth. The color represents the outcome of the collision (either transmission (T) or reflection (R)), and the shape represents the diameter of the droplet. The horizontal spread within each trial was added to aid in visualization.

limitations that these errors could have on our conclusions. Below, I discuss the nature of the experimental errors associated with my measurements.

3.3.1 Droplet Diameter

The droplet diameter measurements were made using the *Tracker* program. Knowing the length (in mm) of another object in the frame, in this case the length of the rhombus cutout inside the tray, we can measure the length of anything else in the frame (in mm). This works by finding the length in mm associated with each pixel in the frame and finding the width in pixels of the droplet. Using this ratio r_{mtp} , we can calculate the length of an object in mm:

$$\frac{\text{length of rhombus in mm}}{\text{length of rhombus pixels}} = r_{mtp} = \frac{\text{diameter of droplet in mm}}{\text{diameter of droplet in pixels}}$$

Since each pixel has a defined length, and because we cannot resolve anything within that pixel, our error is associated with that measurement is at least the width of half

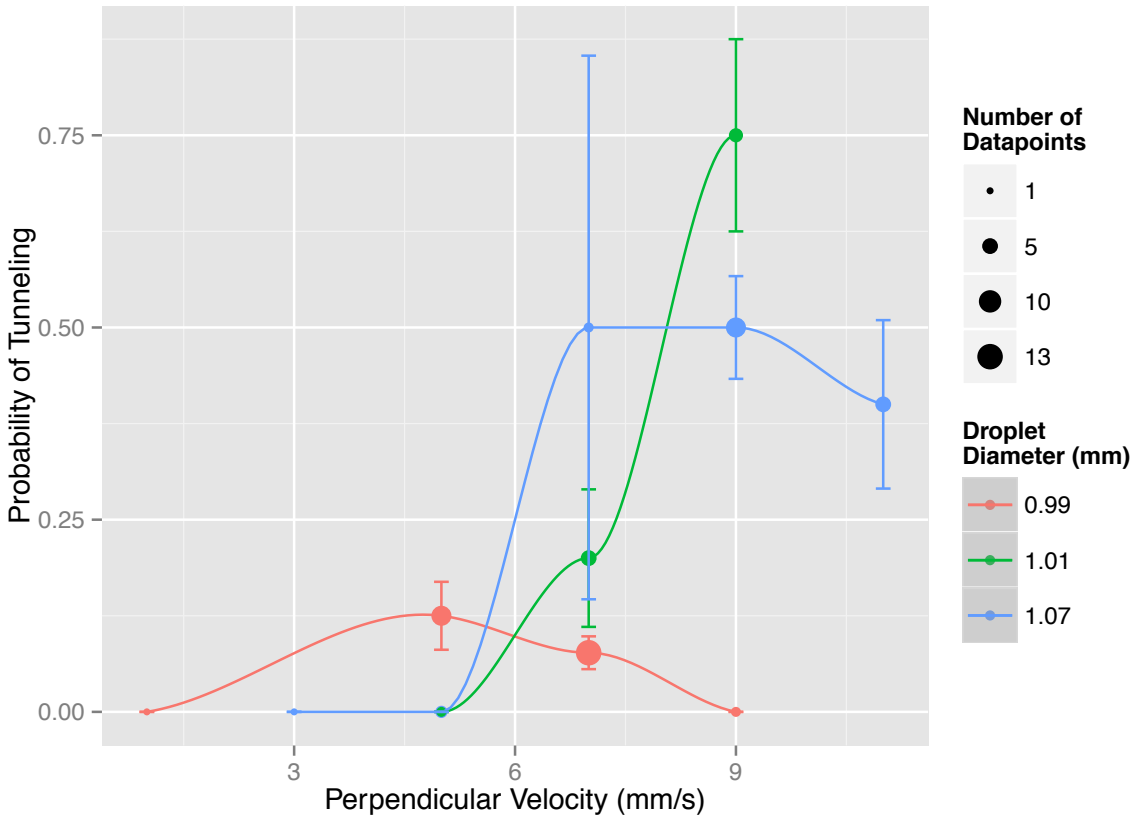


Figure 3.5: Collisions with similar perpendicular velocities were grouped into bins of width 2 mm/s per bin. The overall fraction of transmissions was computed for each bin, and plotted. Colors distinguish between droplet diameters, and sizes indicate the number of data points in each bin. Error bars indicate the associated standard error.

a pixel, usually around **0.04 mm**. There is also an error associated with the initial measurement of the rhombus in pixels, since it can be difficult to discern where exactly each point lies. This error was mitigated by making a new length measurement on *Tracker* every time the barrier was changed.

Additionally, the droplet does not remain a perfect sphere as it bounces. At the bottom of its bounce, the droplet will be squished and appear (from the top view) wider than usual, where at the moment of lift it will be less wide (from the top) than usual. Since the camera recording our data shoots at 24 frames per second, it is impossible to know at what point in the bounce the droplet is, so it is impossible to know when to measure the diameter of the droplet. For this reason, we measured the diameter of the droplet in 3 random frames at each of the 3 barrier heights, and with a total of 9 separate measurements per trial and averaged the results. Because the data for each barrier was filmed separately, this meant computing a new r_{mtp} value for each barrier. For the third trial in which only one barrier was used, the mm to pixel ratio r_{mtp} was re-calculated after 3 diameter measurements, in order to mimic the procedure of the first two trials. In other words, 3 separate groups of 3

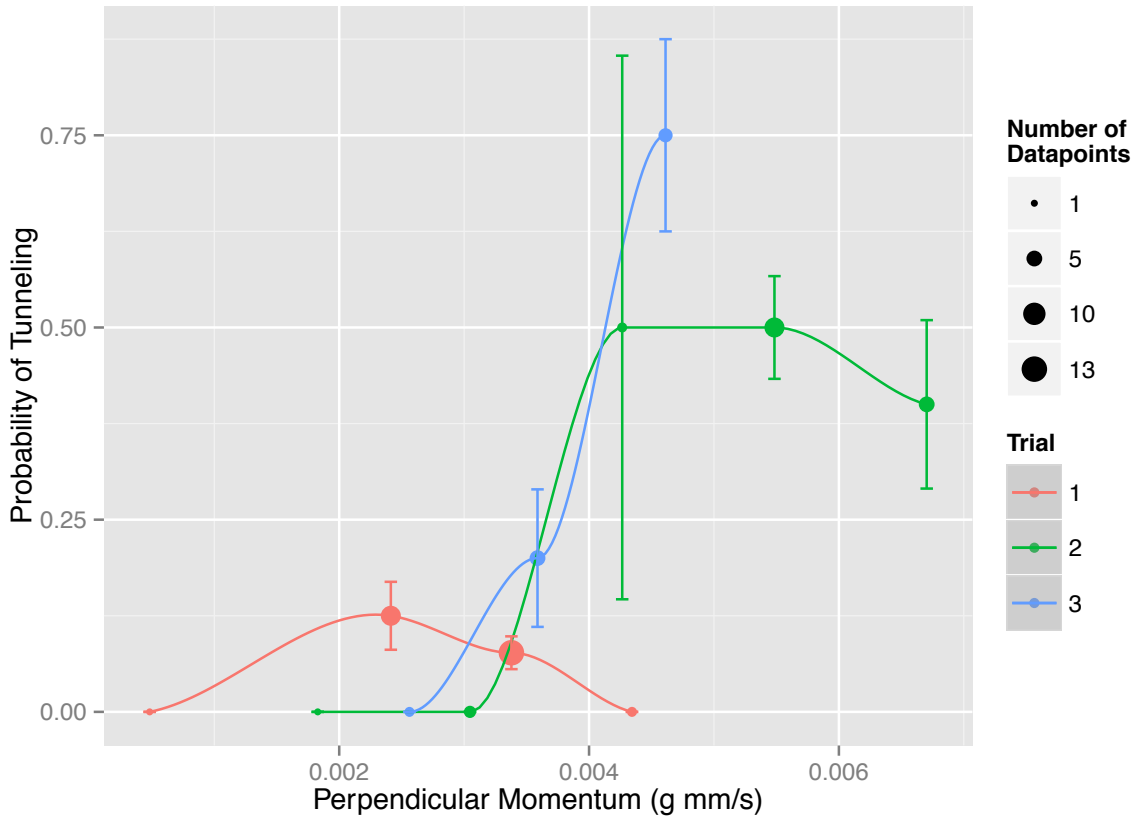


Figure 3.6: Collisions of similar perpendicular momentum were grouped into bins. The overall fraction of transmissions was computed for each bin, and plotted. Colors distinguish between trials, and sizes indicate the number of data points in each bin. Error bars indicate the associated standard error. The droplets were grouped by perpendicular velocities of width 2 mm/s per bin, and then these velocity values were multiplied by m .

measurements were made. Multiple measurements gave us an associated standard error, which combined with the error due to pixel limitations, gave us error bars.

Our measurement procedure helped reduce the error associated with the changing size during a bounce. It also reduced the error associated with finding the exact value of r_{mtp} since it was calculated 3 separate times each trial.

3.3.2 Droplet Velocity

The droplet velocity was measured using *Tracker*. The error in this measurement can be attributed to the Autotracker function, which automatically tracks the motion of the droplet using a built-in algorithm that searches a specific region of a frame for a known arrangement of pixels. Autotracking is mostly spot on, but if left alone for 1,000 frames, the marker begins to deviate from the actual location of the droplet. The marker was adjusted whenever a deviation was noticed. The error can be esti-